

An analysis of elastic scattering reactions with a Fermi-Dirac pomeron opaqueness in impact parameter space

Claude Bourrely

Aix-Marseille Université, Département de Physique,
Faculté des Sciences de Luminy, 13288 Marseille, Cedex 09, France

Abstract

In the Bourrely-Soffer-Wu model (BSW) we introduce for the pomeron a new opaqueness in impact parameter space in terms of different quark contributions described by a Fermi-Dirac distribution. In order to check the validity of this assumption we consider $p p$, $\bar{p} p$, and $\pi^\pm p$ elastic scattering. We emphasize the role of the gluon above the diffraction peak in the differential cross sections. Once these contributions are determined we extend the model to light nuclei elastic reactions like $p d$, $p {}^4\text{He}$ and $\pi^\pm {}^4\text{He}$. The results obtained show a good description of all these elastic processes over the available experimental energy range and moderate momentum transfer.

Key words: elastic hadronic reactions, pomeron, statistical model, light nuclei.

PACS numbers: 13.85.Dz, 11.80Fv, 25.40.Cm, 25.45.De, 25.80.Dj, 12.40.Ee, 14.65.Bt, 25.10.+s

1 Introduction

The advent of the LHC collider has renewed the interest of the high energy behavior of the pp elastic scattering and raises the question of the validity of numerous models devoted to this reaction. Many years ago we proposed the BSW model [1] and made further developments [2]-[4] to improve the agreement with experiments. This model which is based on an impact-picture phenomenology relies for the pomeron contribution to the opaqueness on two assumptions *i)* the energy dependence is deduced from the high-energy behavior of quantum field theory [5, 6] *ii)* the momentum transfer dependence follows from the supposed proportionality between the charge density of the proton and the internal distribution of matter [7, 8]. With these simple assumptions we were able to obtain a good description of the available experimental data obtained at the ISR, SPS and Tevatron.

To be more precise the assumption *ii)* has led us to take for the momentum transfer dependence at the Born level a dipole in an analogous way to the approximation made to describe the proton electromagnetic form factor, however, this was not sufficient and an extra term was added (see next section). We can stress that the relation between charge and matter density was never strictly proven, moreover, in this description we ignore the quark constituents of the proton, so the purpose of the paper is to find a new opaqueness expression which involves the proton constituents. The key observation is that in BSW the opaqueness in impact parameter b space is very similar to a Fermi function, so we propose that for each quarks we associate a Fermi component being dependent on the impact parameter b . An other justification of this new opaqueness is provided by our statistical model for parton distribution functions (PDF) and transverse parton distributions (TMD) which are built in with Fermi functions [9], the model is able to describe a large set of unpolarized and polarized structure functions in momentum space.

This idea to introduce a Fermi function in b space has been considered by several authors [10]-[12] and also in momentum space a Tsallis function [13, 14].¹ However, most of the authors consider a global opaqueness which does not discriminate between the quark components, we will see that in our approach the properties of each of them reflect their importance inside the proton and that their associated thermodynamical potentials remain valid for light nuclei elastic reactions. Let us also mention the Quark-Diquark model [16] and the Generalized Parton Distributions (GPD) which are function of b and the transverse momentum k_T [17].

The paper is organized as follow: after a brief introduction to the original BSW model in sec. 2, we define in sec. 3 a new expression for the opaqueness. In sec. 4 we analyze the pp and $\bar{p}p$ elastic scattering data which determine the free parameters, the relation between the matter distribution and the proton electromagnetic form factor is discussed in sec. 5, then we extend our approach to pd in sec. 6 and to $p^4\text{He}$ elastic scattering in sec. 7. In order to check the validity of our assumption we consider also the πp and $\pi^4\text{He}$ elastic scattering in secs. 8 and 9

¹For a review see Ref. [15].

respectively. The last section contains our conclusion.

2 A summary of the BSW model

In the BSW model [1]-[4] the amplitude is defined by the eikonal expression

$$a(s, t) = \frac{is}{2\pi} \int e^{-i\mathbf{q}\cdot\mathbf{b}} (1 - e^{-\Omega(s, b)}) d\mathbf{b} , \quad (1)$$

where the opaqueness

$$\Omega(s, b) = S(s)F(b) + R(s, b) , \quad (2)$$

the energy dependence is given by the complex crossing symmetric expression deduced from the quantum field theory

$$S(s) = \frac{s^c}{(\ln s)^{c'}} + \frac{u^c}{(\ln u)^{c'}} , \quad (3)$$

in Eq. (2) $F(b)$ is the profile function related to the pomeron contribution and $R(s, b)$ represents Regge contributions which are added to describe the low energy scattering. We define at the Born level the momentum transfer dependence through the product of a dipole multiplied by an extra function whose property is to avoid spurious dips at large momentum transfer in the differential cross sections so the profile function reads

$$\tilde{F}(t) = f[G(t)]^2 \frac{a^2 + t}{a^2 - t} , \quad (4)$$

$$G(t) = \frac{1}{(1 - t/m_1^2)(1 - t/m_2^2)} . \quad (5)$$

We will see that this extra function is in fact related to the gluon contribution. The scattering amplitude is expressed as a Bessel transform

$$a(s, t) = is \int_0^\infty J_0(b\sqrt{-t})(1 - e^{-\Omega(s, b)}) b db , \quad (6)$$

we notice that the factorization property in Eq. (2) does not hold when the amplitude is eikonalized. In impact space the profile function reads

$$F(b) = \int_0^\infty \tilde{F}(t) J_0(b\sqrt{-t}) \sqrt{-t} d\sqrt{-t} , \quad (7)$$

where the Bessel transform of $\tilde{F}(t)$ gives the dimensionless expression

$$\begin{aligned}
F(b) = & -fm_1^2m_2^2 \left\{ [1 + 2a^2A_{13}] A_{12}^2m_2^2 \frac{m_1b}{2} K_1(m_1b) \right. \\
& + [1 + 2a^2A_{23}] A_{12}^2m_1^2 \frac{m_2b}{2} K_1(m_2b) \\
& + [2 + 2a^2(A_{13} + A_{23})] A_{12}^3m_1^2m_2^2 (K_0(m_1b) - K_0(m_2b)) \\
& + 2a^2m_1^2m_2^2A_{12}A_{32}A_{31} \times \\
& \left. \times [A_{31} (K_0(m_1b) - K_0(ab)) - A_{32} (K_0(m_2b) - K_0(ab))] \right\}, \quad (8)
\end{aligned}$$

the coefficients A_{ij} depend on m_1 , m_2 , a . In Eq. (8) the terms associated with the Bessel $K_0(ab)$ which depend on the parameter a introduced in (4) give a negative contribution to the sum. Conversely

$$\tilde{F}(t) = \int_0^\infty F(b) J_0(b\sqrt{-t}) b db. \quad (9)$$

A fit of experimental data gives for the pomeron parameters the values [3]

c	$=$	0.167,	c'	$=$	0.748
m_1	$=$	0.577 GeV,	m_2	$=$	1.719 GeV
a	$=$	1.858 GeV,	f	$=$	6.971 GeV ⁻²

Table 1: Parameters of the BSW model.

3 The Fermi-Dirac opaqueness

At the level of the BSW Born term in momentum space we used a modified dipole approximation arguing that there should be some kind of similarity between the distribution of matter and the distribution of charge inside the proton. Taking the Fourier transform of this modified dipole we get the opaqueness $\Omega(s, b)$ in the impact parameter space b . Now, looking at the curve $F(b)$ in Fig. 2 of Ref. [1], we observe that its shape can be approximated by Fermi-Dirac functions.

We know from QCD that inside a proton its constituents are 2 quarks u , one d , a sea and the gluon, we can infer that each of them contribute to the profile function $F(b)$ and from our previous observation we deduce that their global effect can be described by a Fermi function, so we make the hypothesis that the individual nature of these constituents is also of Fermi type and that the sum should reproduce the same profile function $F(b)$ as in BSW.

Now, in analogy with the Fermi PDF expressions which in Q^2 , x space depend on thermodynamical potentials and a temperature, see Ref. [9], we propose to associate to each quark a Fermi function with a thermodynamical potential now in

b space, namely, X_u , X_d , $X_{\bar{q}}$, X_g , and a parameter b_0 which represents an average size localization of the partons inside the proton. For the gluon due to the boson nature we use a Bose-Einstein function and introduce a non zero potential otherwise its contribution would be infinite for $b = 0$. These properties can be summarized by the following crossing symmetric expression

$$F(b) = c_0 \left[\frac{1}{1 + \exp\left[\frac{b-X_d}{b_0}\right]} + \frac{c_1}{1 + \exp\left[\frac{b-X_u}{b_0}\right]} + \frac{c_2}{1 - \exp\left[\frac{b+X_g}{b_0}\right]} + \frac{c_3}{1 + \exp\left[\frac{b+X_{\bar{q}}}{b_0}\right]} \right], \quad (10)$$

where the signs in front of the potentials are defined according to the same convention as in the case of parton distributions. Here, c_0 plays the role of the parameter f in BSW, the coefficients c_1 , c_2 and c_3 are the relative weight of u , g and sea with respect to the quark d . We ignore in this first approach heavy quarks.

Our goal is to show that the expression (10) can be used to describe different elastic reactions and that once the potentials are determined from $p p$ elastic scattering their values are an *intrinsic property of the quarks* also valid for scattering reactions involving light nuclei and give a reliable description of the proton electric form factor at low Q^2 .

4 The $p p$ and $\bar{p} p$ elastic scattering

Now, it remains to determine the values of the above parameters by making a fit of the data. We use the same set of data as in the original BSW [24]-[37], precisely, the energy ranges from $p_{lab} = 100$ GeV to $\sqrt{s} = 1.8$ TeV for $p p$ and $\bar{p} p$, and for the momentum transfer we restrict the values to $|t| < 5$ GeV². In order to put more constraints on the pomeron we take into account low energy data so we use for the Regge contributions the same expressions as in BSW [1, 3]. A fit gives for the pomeron parameters the following numerical values, Table 2:

c	$= 0.1677 \pm 0.0018,$	c'	$= 0.7103 \pm 0.0176$
c_0	$= 0.0891 \pm 0.0029,$	c_1	$= 13.4678 \pm 0.238$
c_2	$= 21.6197 \pm 0.358,$	c_3	$= 4.9707 \pm 0.242$
b_0	$= 0.3337 \pm 0.0098$ fm,	X_u	$= 0.269 \pm 0.0073$ fm
X_d	$= 1.0654 \pm 0.011$ fm,	$X_{\bar{q}}$	$= 1.8837 \pm 0.03138$ fm
X_g	$= 0.6832 \pm 0.014$ fm		

Table 2: Pomeron parameters of the Fermi model for $p p$ and $\bar{p} p$ elastic scattering.

With these parameters we obtain a $\chi^2 = 2060$ for 955 pts which gives a $\chi^2/pt = 1.95$ and has to be compared with BSW value $\chi^2/pt \sim 2.8$. We notice that the parameters c , c' are close to the ones obtained with BSW which means that the asymptotic behavior of $S(s)$ is preserved.

We show in Fig. 1 the function $\tilde{F}(t)$ and in Fig. 2 the profile function $F(b)$ produced by the Fermi-Dirac functions both of them are very close to the BSW curves. With the parameters of Table 2 the individual contribution of quarks to the profile function is shown in Fig. 3, we see that they are concentrated around 1 fermi which is the expected size of the proton, the two quarks u in the proton give the main contribution compared to the d quark, the gluon has a contribution concentrated at small b .

We plot in Figs 4-5 the differential cross sections for $p p$ and $\bar{p} p$ where we obtain a good agreement with the data. A prediction at $\sqrt{s} = 7$ TeV shows that the Fermi version presents as BSW the same mismatch at large t when compared with the TOTEM differential cross section measurement [18], see Fig. 6. At this energy we predict $\sigma_{tot} = 91.95 \pm 1.2$ mb, $\sigma_{el} = 25.7 \pm 2.2$ mb, $\rho = 0.124$, these values have to be compared with the TOTEM data $\sigma_{tot} = 98.0 \pm 2.5$ mb, notice that we agree with $\sigma_{el} = 25.43 \pm 1.07$ mb and the position of the first minimum of the differential cross section, we show in Fig. 7 the behavior of the total and elastic cross sections.

Let us make a comment: the inclusion the TOTEM data in our fit notably increase the χ^2 , so the quoted parameters values are obtained leaving aside these data. A discussion of the BSW model with respect to the TOTEM data is reported in Ref. [19]. In fact, our pomeron whose energy dependence is controlled by the parameters c, c' which are constrained by a fit in an energy range from low energy up to 1.8 TeV cannot give a total cross section as high as the one obtain by TOTEM. In order to reach this value we need a revision of the pomeron behavior, but before doing any modification we wait for a confirmation from an other experiment [20]. Let us point out that at the Tevatron energy 1.8 TeV we obtain $\sigma_{tot} = 73.6 \pm 1.5$ mb which is in agreement within the experimental range $71.42 \leq \sigma_{tot} \leq 80.03$ mb with an average error 2.4 mb [21]-[23]. Notice that the values of the above parameters c, c' are perfectly compatible with the high energy behavior of light nuclei reactions discussed in the next sections.

The role of the gluon

In the Born term Eq. (4) of BSW we have introduced the extra term $\frac{a^2+t}{a^2-t}$ in order to cancel a spurious second dip in the differential cross section, this term implies that $\tilde{F}(t)$ has a zero at $|t| = a^2 = 3.74$ GeV² and becomes negative above. The Bessel transform of the Fermi distribution (10) with respect to b gives a function $\tilde{F}(t)$ which has also a zero at $|t| = 4.3$ GeV² and a negative value above, see Fig. 1. We will show that the origin of this zero is produced in fact by the gluon as we now explain.

Looking at the expression of $F(b)$ Eq. (10) it contains 4 terms including the u, d , the sea and the gluon contributions, let us suppose that we remove the gluon contribution, a fit made with only the u and d and the sea gives a very large χ^2 , moreover, $\tilde{F}(t)$ has no zero, so one can conclude that the gluon contribution is necessary to obtain a reasonable χ^2 and to produce a zero in $\tilde{F}(t)$. Concerning the gluon a more detailed comparison between the Fermi and the BSW approaches can be made. When making a plot of Eq. (8) we observe that the terms associated with

Bessel functions whose arguments depends on m_1 or m_2 give a positive contribution to $F(b)$, while terms associated with the parameter a give a negative contribution. In the Fermi case the gluon has a denominator $1 - \exp[\frac{b+X_g}{b_0}]$ where the minus sign reflects the Bose nature of the contribution, now the value of the potential X_g must be such that the denominator never vanishes otherwise we get a singularity, taking also into account the constraint for $b = 0$ we see that the denominator must be always negative which makes a clear correspondence between the gluon and the contribution due to the term associated with the parameter a in BSW.

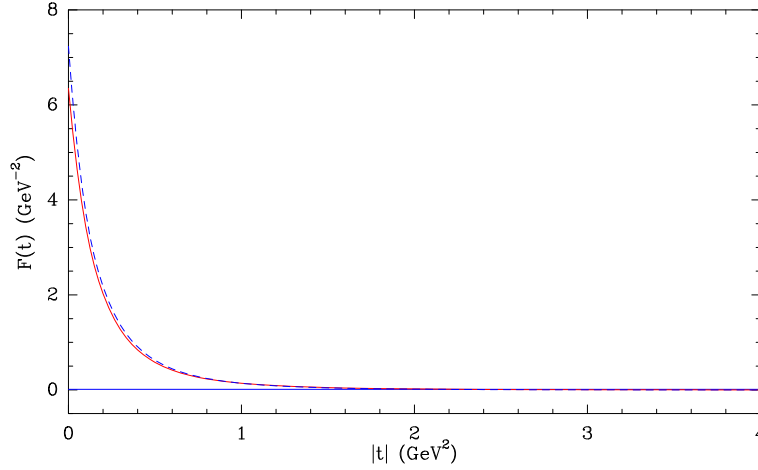


Figure 1: The profile function $\tilde{F}(t)$ as a function of $|t|$ for $p - p$ scattering. Fermi solid red curve, BSW dashed blue curve.

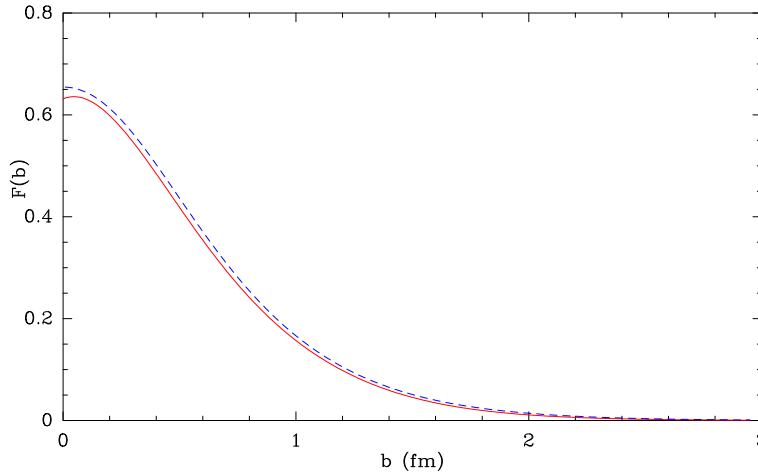


Figure 2: The profile function $F(b)$ as a function of b for $p - p$ scattering. Fermi solid red curve, BSW dashed blue curve.

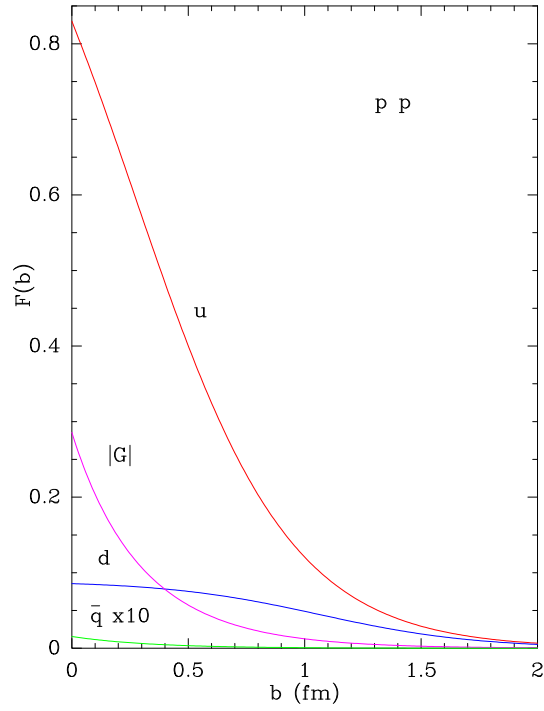


Figure 3: Individual contribution of quarks to the profile function for $p-p$ scattering.

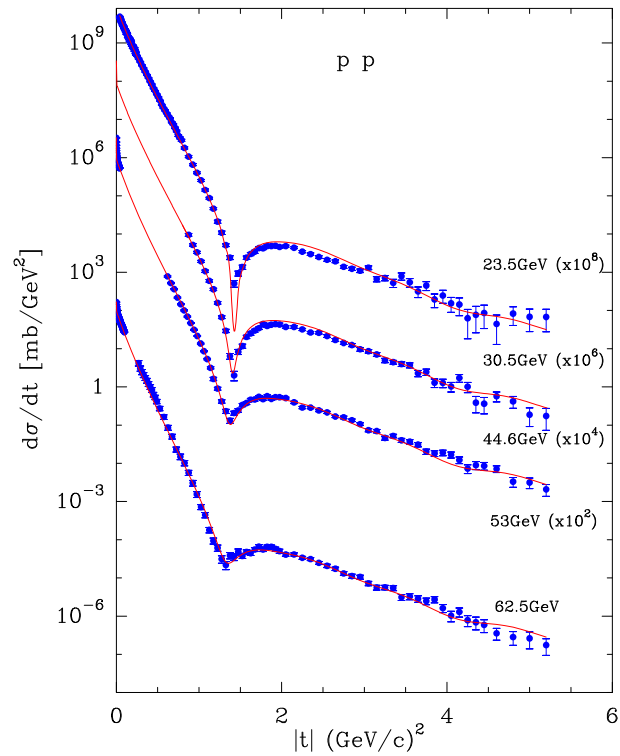


Figure 4: The pp differential cross section as a function of $|t|$. Experiments from Refs. [24]-[29].

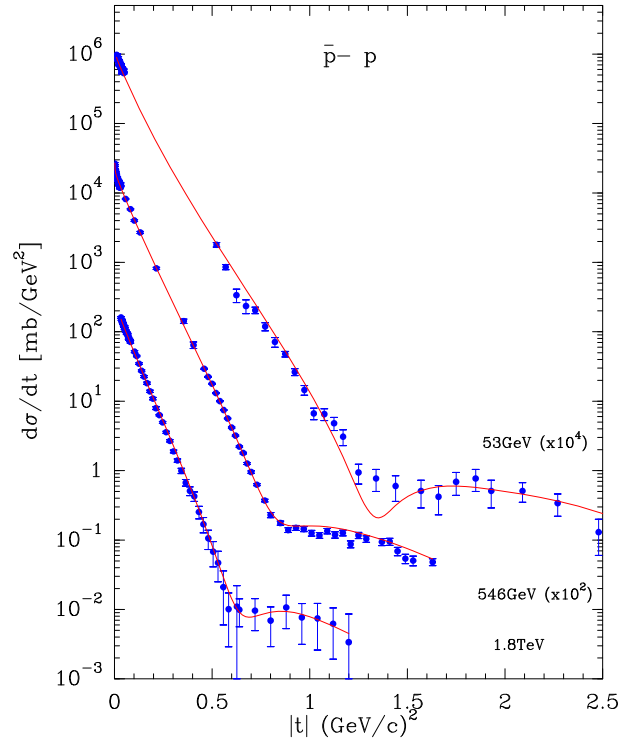


Figure 5: The $\bar{p}p$ differential cross section as a function of $|t|$. Experiments from Refs. [27, 28], [30]-[37].

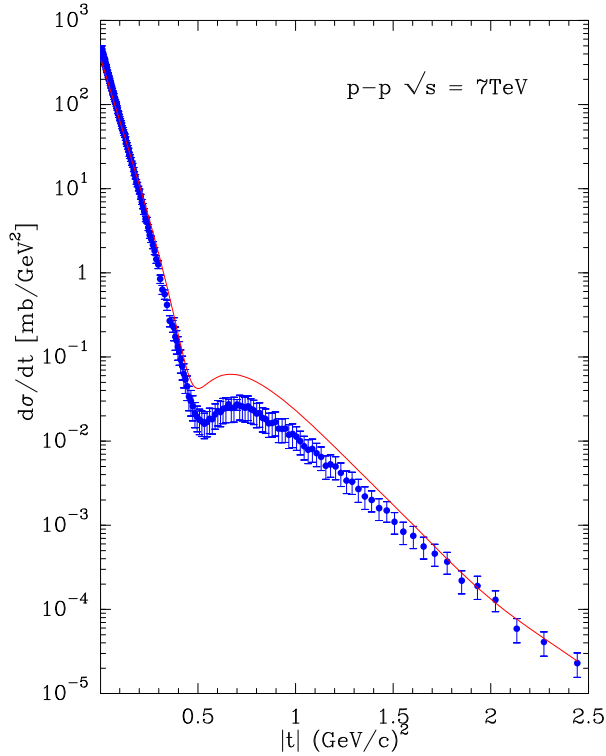


Figure 6: A prediction of the Fermi model compared to the TOTEM experimental data [18].

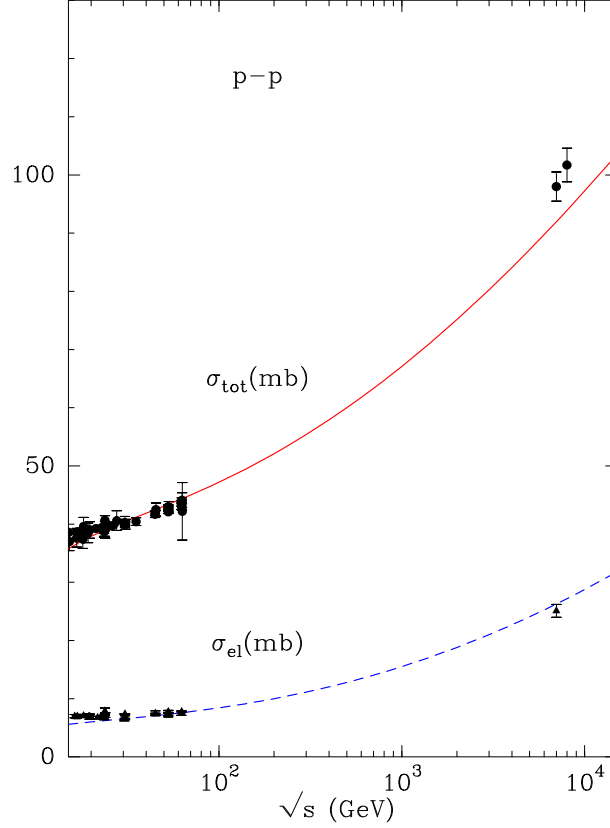


Figure 7: The p-p total and elastic cross sections as a function of \sqrt{s} . Experimental data from Refs. [18, 38].

5 The proton electric form factor at low Q^2

In section 2, we have introduced the BSW profile function $\tilde{F}(t)$ Eq. (4) which depends on $G^2(t)$ (Eq. 5) interpreted as a nuclear form factor. In section 3, we have defined a new $\tilde{F}(t)$ as the Bessel transform of the Fermi-Dirac expressions (10). Now, we raise the question if there is any relation between this nuclear form factor and the electromagnetic form factor of the proton. To this end, we define using Eq. (10) the proton electric form factor by the expression

$$\begin{aligned}
 G_e^2(Q^2) = & \int_0^\infty b db J_0(bQ) f_e^2 \left[\frac{1}{1 + \exp\left[\frac{b-X_d}{b_e}\right]} + \frac{c_1}{1 + \exp\left[\frac{b-X_u}{b_e}\right]} \right. \\
 & \left. + \frac{c_2}{1 - \exp\left[\frac{b+X_d}{b_e}\right]} + \frac{c_3}{1 + \exp\left[\frac{b+X_{\bar{q}}}{b_e}\right]} \right]. \quad (11)
 \end{aligned}$$

Compared to Eq. (10) we introduce the normalization factor f_e^2 and replace the quarks extension b_0 inside the proton by b_e which corresponds to the electromagnetic case, all the other parameters are kept fixed at the values given in Table 2. The normalisation factor f_e^2 is determined by the condition $G_e(0) = 1$, we obtain $f_e^2 = 0.0143 \text{ GeV}^2$ and the best agreement with the experimental form factor data gives $b_e = 0.326 \text{ fm}$ a value slightly less than $b_0 = 0.337 \text{ fm}$, we can interpret this small difference from the fact that u quarks give the most important contribution at small b (see Fig. 3) and carry 4/3 of the charge while the d quark giving a smaller contribution has a charge -1/3.

In order to make a comparison with experiment we have to rely on the available measured ratio $G_e(Q^2)/G_{dipole}(Q^2)^2$ since we are not able to compute the magnetic form factor, so we cannot use the measurements G_e/G_m . In Fig. 8 we show the plot $G_e(Q^2)/G_{dipole}(Q^2)$ produced by the Fermi distributions (11) (solid line), the agreement with experimental data at low Q is relatively good, we notice that the recent polarized experiment at JLab [39] (squares in the figure) gives the most precise values. For reference we show the case of BSW given by Eq. (4) we observe a fast decrease of this ratio because the parameters m_1 and m_2 are only valid in the nuclear case.

In the introduction we raised the question of a possible relation between the nuclear and electromagnetic form factors, our Fermi approach shows clearly that with only two new parameters we can make a close link between the distribution of matter and the distribution of charge inside the proton.

6 The $p d$ elastic scattering

In the previous section we considered the elastic scattering between two elementary particles $p p$, $\bar{p} p$ and found the basic properties of quarks, sea and gluon interaction through a Fermi-Dirac function in impact parameter space. The question arises how to extend this type of interaction when a light nucleus like the deuteron is involved in the $p d$ elastic scattering.

Our theoretical input for the profile function is the same formula defined for $p p$ by Eq. (10) where we keep the same value of the parameters c, c' and the thermodynamical potentials, the only free parameters are the normalization coefficients c_0, c_1, c_2, c_3 , and the parameter b_0 associated with the deuteron size, we infer that since the total cross section for this process is higher than in the proton case c_0 must increase.

The experimental data [44]-[46] cover the energy range $40 \leq p_{lab} \leq 397 \text{ GeV}$ and the momentum transfer range $0.00077 \leq |t| \leq 0.2435 \text{ GeV}^2$ [44]-[46]. Of course, the energy domain is more limited than in the $p p$ reaction, and the momentum transfer covers only low $|t|$ values, nevertheless, we find interesting to check the validity of our assumption on the universality of the thermodynamical potentials in

² $G_{dipole}(Q^2) = \frac{1}{(1+Q^2/0.71)^2}$ is the usual dipole form factor.

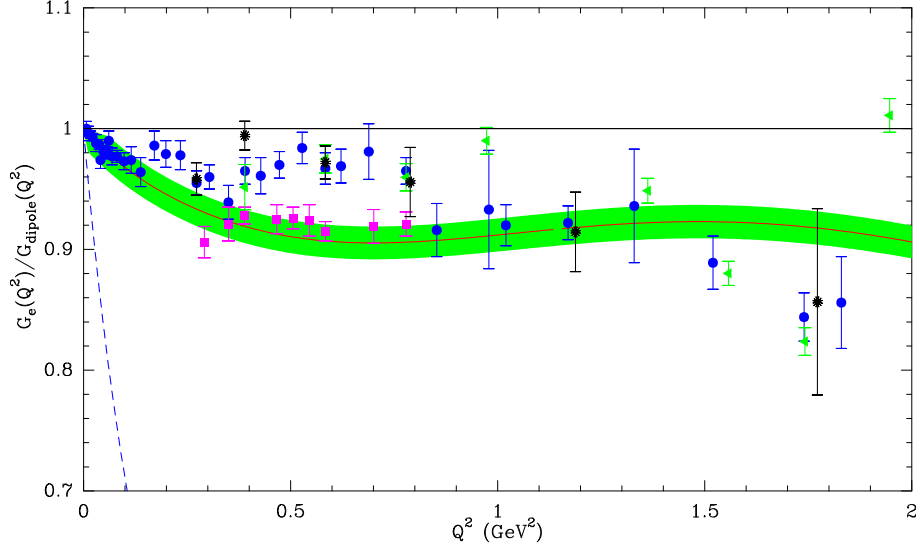


Figure 8: The proton electric form factor $G_e(Q^2)$ normalized to G_{dipole} as a function of Q^2 . Fermi solid curve, uncertainty domain shaded area, BSW dashed curve. Experimental data: square [39], triangle [40], star [41], circle a data analysis presented in Ref. [42].

this case. After a fit of data we obtain a $\chi^2 = 1533$ for 1000 pts giving a $\chi^2/pt = 1.53$ which is slightly better than the proton value. The resulting parameters for the pomeron are given in Table 3.

$c_0 = 0.0726 \pm 0.002,$	$c_1 = 33.1219 \pm 0.229$
$c_2 = 7.4228 \pm 0.0.23,$	$c_3 = -35.592 \pm 1.09$
$b_0 = 0.544 \pm 0.0122 \text{ fm},$	

Table 3: Pomeron parameters of the Fermi model for $p d$ elastic scattering.

The profile function $F(b)$ shown in Fig. 9 differs from the $p p$ case with a maximum at $b = 0.5 \text{ fm}$. In Fig. 10 we plot the different components of the pomeron contribution, we observe that the gluon and the quark u give the major contribution. The differential cross sections show a perfect agreement with the data in the measured low t region, see Figs. 11-12. Concerning the total cross we obtain for instance at $E_{lab} = 240 \text{ GeV}$, $\sigma_{tot} = 73.77 \pm 0.4 \text{ mb}$ to be compared with the experimental value $74.42 \pm 0.53 \text{ mb}$ [43]

This result confirms that our basic Fermi interaction between quarks obtained in the elastic proton case where we have a system made of $4u + 2d$ remains valid for this light nucleus scattering where now it contains $5u + 4d$.

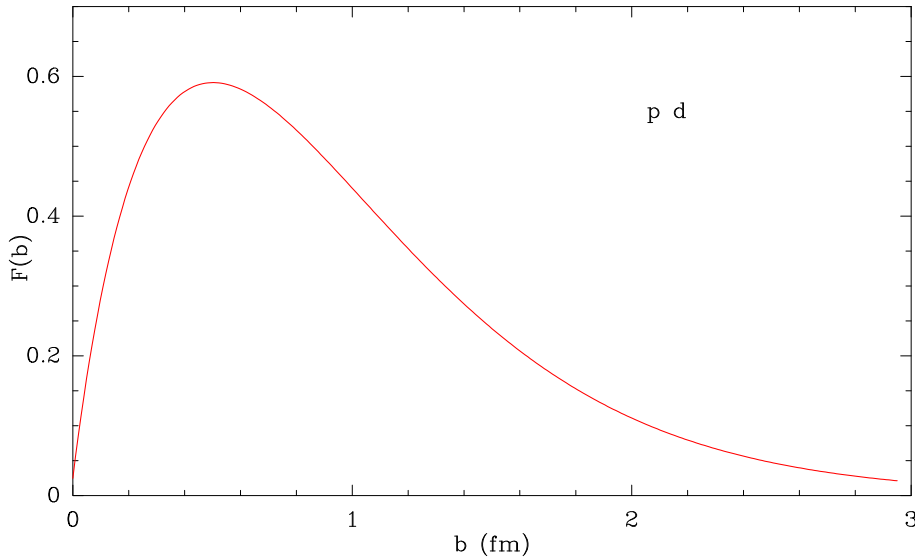


Figure 9: The profile function $F(b)$ as a function of b .

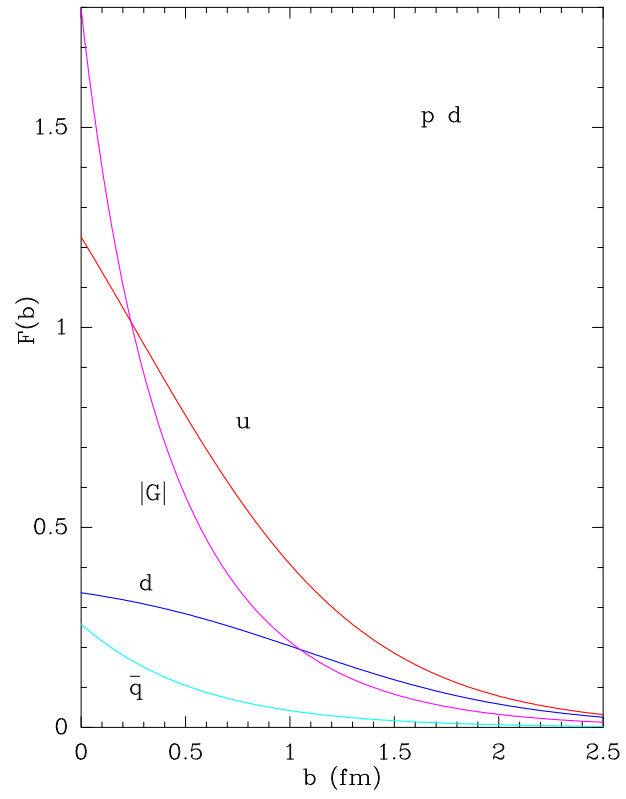


Figure 10: Individual contribution of quarks to the profile function for $p - d$.

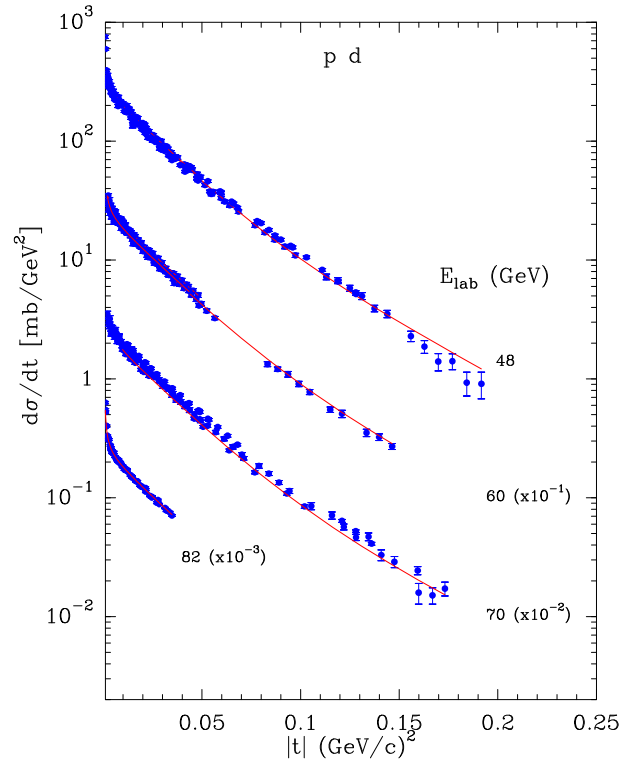


Figure 11: The pd differential cross section as a function of $|t|$. Experiments from Refs. [44]-[46].

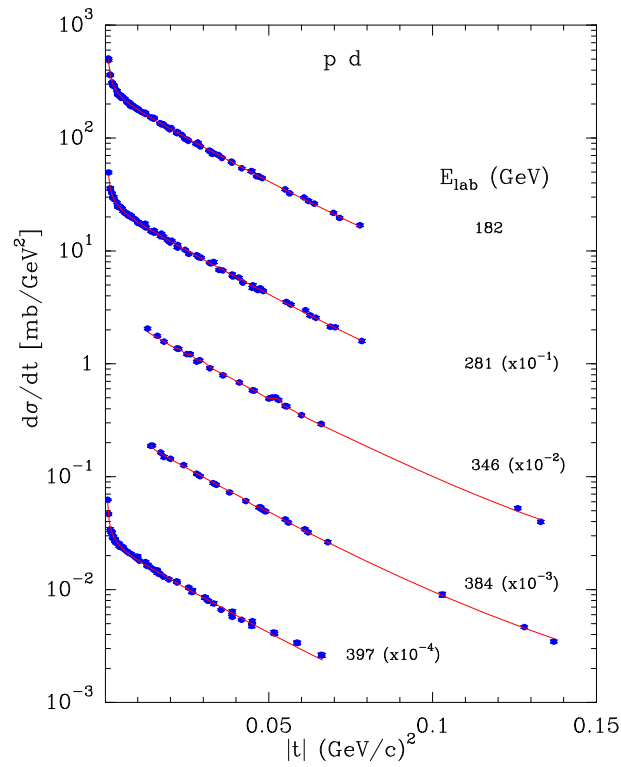


Figure 12: The pd differential cross section as a function of $|t|$ continued.

7 The p ^4He elastic scattering

Following the same approach of the previous sections, we propose to describe the elastic reaction p ^4He from the measurements made at Fermilab with a gas target in a range of energies from 97 to 400 GeV and momentum transfer $0.003 \leq |t| \leq 0.52 \text{ GeV}^2$ [47, 48].

Our theoretical input for the profile function relies on the same formula defined for p p by Eq. (10) where we keep the same value of the parameters c, c' and the thermodynamical potentials, here again the only free parameters are the coefficients c_0, c_1, c_2, c_3 and the parameter b_0 .

A fit gives a $\chi^2 = 476$ for 504 pts or a $\chi^2/pt = 0.94$. The resulting parameters for the pomeron are given in Table 4:

c_0	$=$	$0.0134 \pm 0.0015,$	c_1	$=$	29.9041 ± 1.01
c_2	$=$	$24.9568 \pm 1.02,$	c_3	$=$	0.4968 ± 0.067
b_0	$=$	$0.5967 \pm 0.0018 \text{ fm}$			

Table 4: Pomeron parameters of the Fermi model for p ^4He elastic scattering.

With these parameters we plot in Fig. 13 the different components of the pomeron contribution, we observe that the gluon and the quark u give the major contribution a situation similar to the p d case (see Fig. 10). A plot of the differential cross sections is shown in Fig. 14, we notice that the dip region is well described, concerning the total cross we obtain at $E_{lab} = 250 \text{ GeV}$ $\sigma_{tot} = 132.13 \pm 0.5 \text{ mb}$ to be compared with $\sigma_{tot} = 131.6 \pm 0.8 \text{ mb}$ of Ref. [48]. For this reaction the agreement with the data validates our assumption on the structure of the profile function $F(b)$ and the fact that the thermodynamical potentials are kept the same.

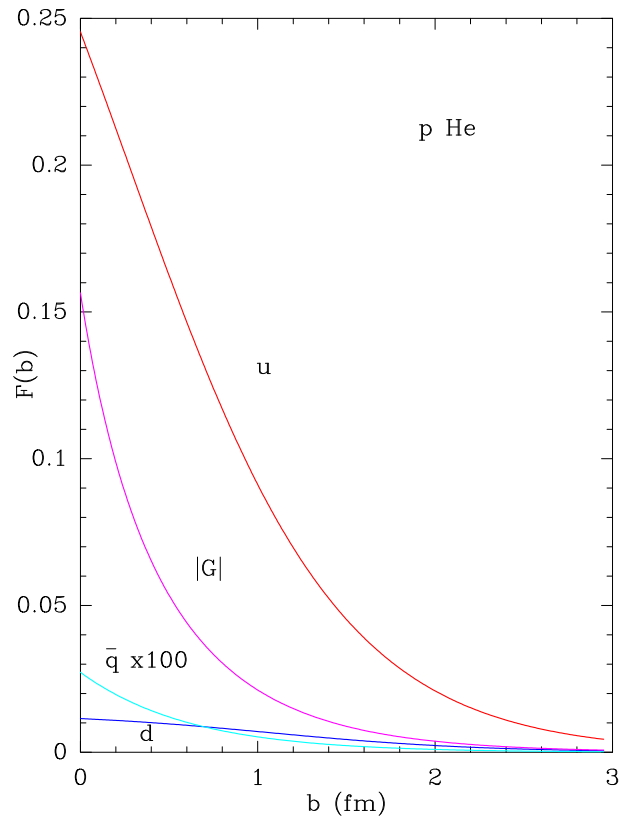


Figure 13: Individual contribution of quarks to the profile function for $p\ ^4\text{He}$.

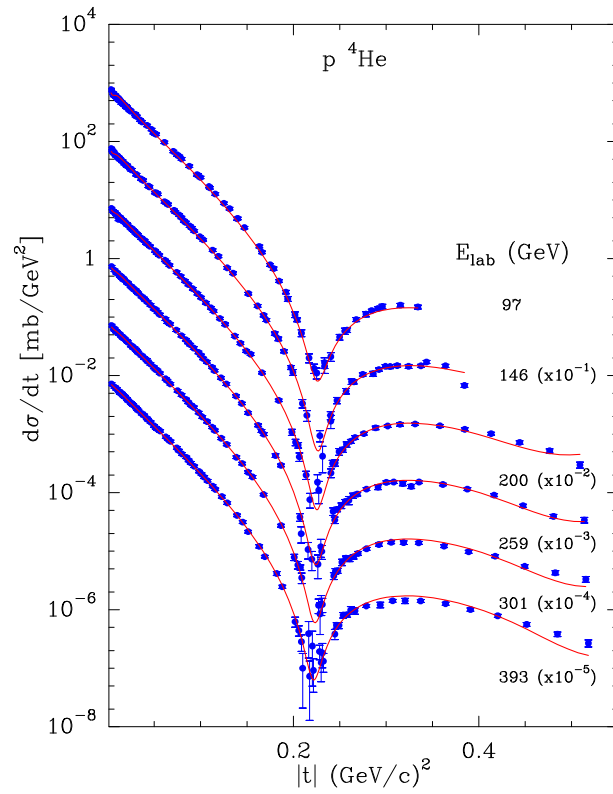


Figure 14: The $p\ ^4\text{He}$ differential cross section as a function of $|t|$. Experiments from Refs. [47, 48].

8 The $\pi^\pm p$ elastic scattering

In addition to $p p$ scattering the $\pi^\pm p$ must give new informations on the partons content of the πp interaction. For this reaction, in the original BSW the pomeron contribution is defined by the expression:

$$\tilde{F}(t) = f_\pi G(t) \mathcal{F}_\pi(t) \frac{a_\pi^2 + t}{a_\pi^2 - t}, \quad (12)$$

where $\mathcal{F}_\pi(t) = \frac{1}{1-t/m_{3\pi}^2}$ is a simple pole, from a fit we obtained the following parameters

$$m_{3\pi} = 0.7665 \text{ GeV}, \quad f_\pi = 4.2414, \quad a_\pi = 2.3272 \text{ GeV}. \quad (13)$$

For the Fermi description of the πp interacting system in impact parameter space we explore a slightly different approach compared to the proton case, in the sense that we introduce a different quark potential according to the charge of the pion so that the new pomeron profile function takes the form

$$F_\pi^\pm(b) = d_0 \left[\frac{1}{1 + \exp\left[\frac{b-X_d^\pm}{b_0}\right]} + \frac{d_1}{1 + \exp\left[\frac{b-X_u^\pm}{b_0}\right]} + \frac{d_2}{1 - \exp\left[\frac{b+Z_g}{b_0}\right]} + \frac{d_3}{1 + \exp\left[\frac{b+Z_{\bar{q}}}{b_0}\right]} \right]. \quad (14)$$

Since the quark structure for π^+ is $u \bar{d}$ and for π^- is $d \bar{u}$, we define a set of thermodynamical potentials X_u^\pm , X_d^\pm corresponding to π^\pm , the reason being that in the system at rest we have $3u + d$ for π^+ and $2u + 2d$ for π^- so the potentials are not necessarily to be the same as in $p p$. For the sea we introduce a global potential $Z_{\bar{q}}$, and for the gluon component a potential Z_g . The parameters c , c' which drive the asymptotic energy behavior are kept the same as in $p p$ (see Table 2).

A simultaneous fit of π^\pm data for $p_{lab} = 100 - 250$ GeV, and momentum transfer $|t| < 2.5$ GeV² [49]-[53], gives a $\chi^2 = 1005$ with 608 pts or a $\chi^2/pt = 1.65$. The resulting parameters for the pomeron are given in Table 5.

d_0	$= 3.4408 \pm 0.118,$	d_1	$= 2.406 \pm 0.21$
d_2	$= 2.5345 \pm 0.195,$	d_3	$= 5.5128 \pm 0.323$
X_u^+	$= 0.2802 \pm 0.002 \text{ fm},$	X_u^-	$= 0.2307 \pm 0.0197 \text{ fm}$
X_d^+	$= 0.0096 \pm 0.0004 \text{ fm},$	X_d^-	$= 0.1772 \pm 0.0065 \text{ fm}$
$Z_{\bar{q}}$	$= 0.6323 \pm 0.0118 \text{ fm},$	Z_g	$= 0.3537 \pm 0.0116 \text{ fm}$
b_0	$= 0.3096 \pm 0.004 \text{ fm}$		

Table 5: Pomeron parameters of the Fermi model for $\pi^\pm p$ elastic scattering.

Notice that the parameters $d_0, d_1, d_2, d_3, b_0, Z_{\bar{q}}, Z_g$ are the same for both reactions. In Figs. 15-16 a plot is made for $\tilde{F}(t)$ and $F(b)$ with a comparison to the BSW profile, the curves are very close which shows the validity of the Fermi profile. The variation of $\tilde{F}(t)$ in πp for BSW shows a zero at $|t| = 5.6$ GeV² while for Fermi

the zero occurs at $|t| = 6.9 \text{ GeV}^2$, this difference in the zero position reflects the dominance of the gluon over the sea as seen in Fig. 17.

Compared to $p p$ scattering we have not the same range of high energy data so the pomeron parameters are subject to less constraints, nevertheless it is interesting to determine the size of the different components in Eq. (14). With the parameters of Table 5 we plot in Fig. 17 the individual contribution of the components in the $\pi^+ p$ case, we observe the dominance of the quark u and the gluon, but the sea contribution which was small in $p p$ (see Fig. 3) becomes more sizeable which is expected due to the pion effect.

We have introduced In Eq. (14) the potentials X_u^\pm , X_d^\pm in order to separate the reactions π^\pm leading to two separated profiles $F_\pi^\pm(b)$, with the parameters of Table 5 the numerical difference between $F_\pi^+(b)$ and $F_\pi^-(b)$ is very small, this fact can be explained by the experimental the differential cross sections for the two processes which are close in the energy range considered here, we remark that the difference is in part due to the Regge ρ contribution.

In Figs 18-19 a plot of the differential cross sections shows a reasonable agreement with the data. Also, the large $|t|$ values presented in Fig. 20 reveal the existence of a dip around $|t| = 4.5 \text{ GeV}^2$ consistent with the data. For the total cross sections we obtain at $p_{lab} = 310 \text{ GeV}$ a value $\sigma_{tot} = 24.86 \pm 0.2 \text{ mb}$ for $\pi^- p$ and $\sigma_{tot} = 24.48 \pm 0.3 \text{ mb}$ for $\pi^+ p$, the experimental values are respectively $\sigma_{tot} = 24.9 \pm 0.08 \text{ mb}$ and $\sigma_{tot} = 24.5 \pm 0.1 \text{ mb}$ from Ref. [43]. Since we have a different pomeron potential for π^- and π^+ what is the incidence on the total cross section at high energy, a prediction at $\sqrt{s} = 7 \text{ TeV}$ gives respectively for the two reactions 58.8 mb and 58.2 mb, the difference is 1%, so the near equality of the cross sections at high energy is preserved in accordance with the Pomernanchuk theorem.

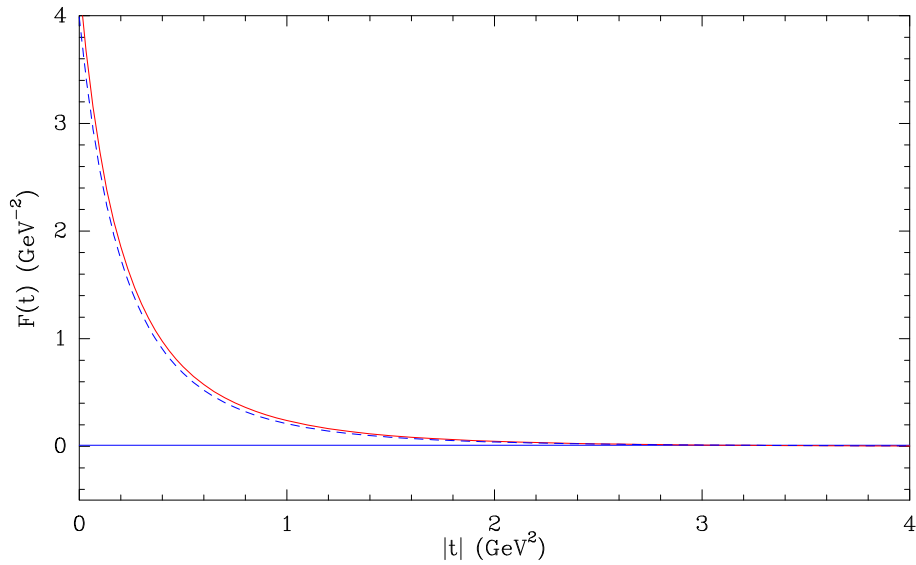


Figure 15: The profile function $\tilde{F}(t)$ as a function of $|t|$ for $\pi^\pm p$. Fermi solid red curve, BSW dashed blue curve.

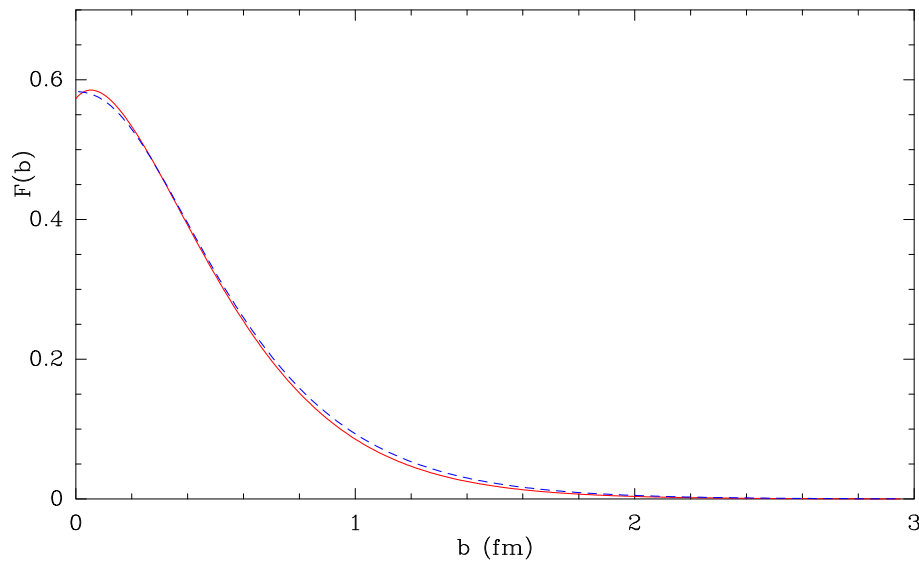


Figure 16: The profile function $F(b)$ as a function of b for $\pi^\pm p$. Fermi solid red curve, BSW dashed blue curve.

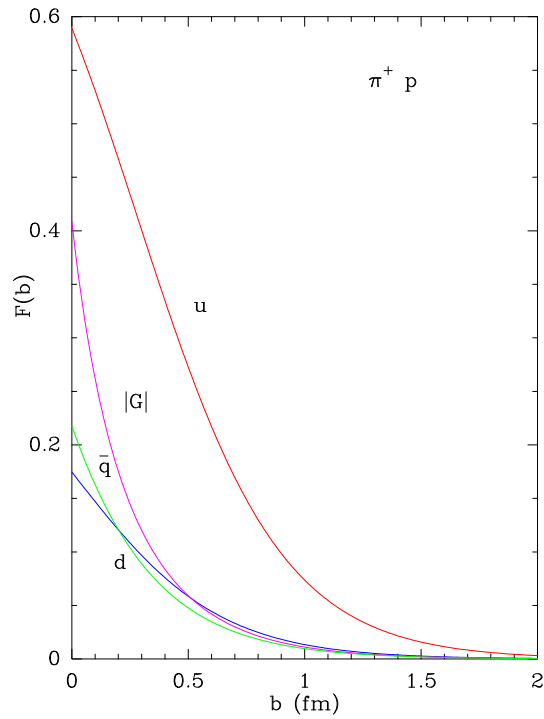


Figure 17: Individual contribution of quarks to the profile function for $\pi^\pm p$.

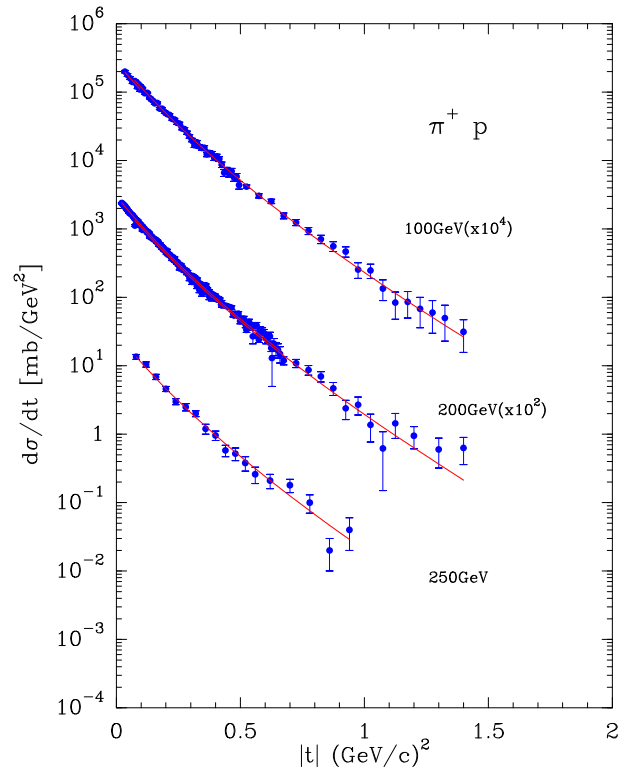


Figure 18: The $\pi^+ p$ differential cross section as a function of $|t|$. Experiments from Refs. [49]-[53].

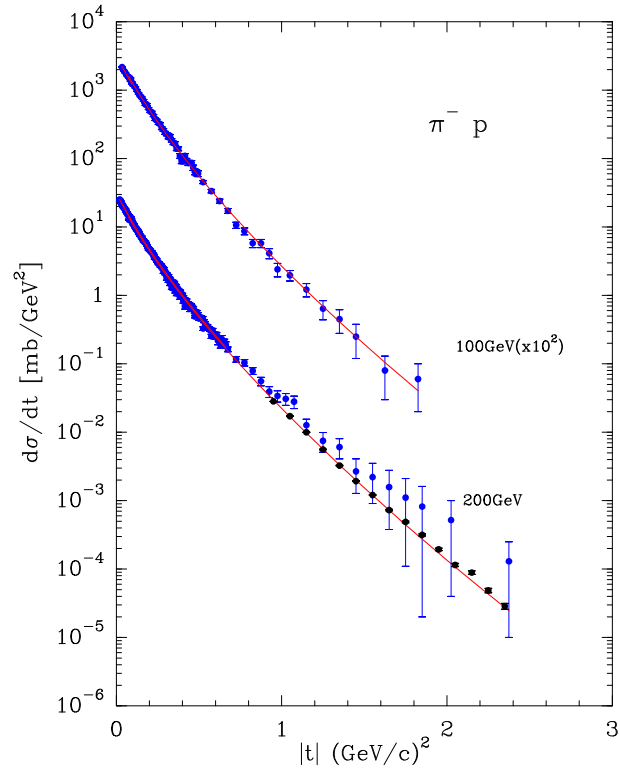


Figure 19: The $\pi^- p$ differential cross section as a function of $|t|$. Experiments from Refs. [49]-[52].

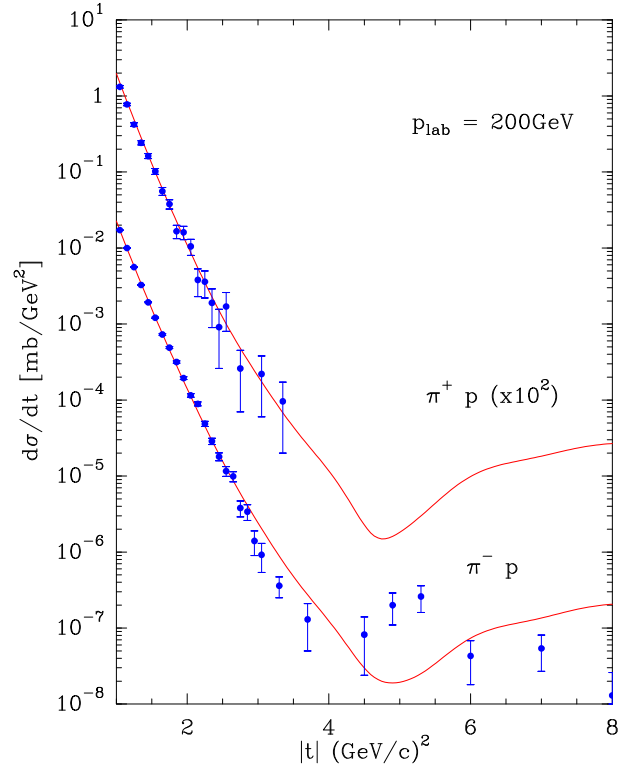


Figure 20: The $\pi^\pm p$ differential cross section for large $|t|$ values. Experiment from Ref. [50]

9 The π^\pm ^4He elastic scattering

To study this reaction we follow the same approach as in the previous sections, namely, we keep the parameters c , c' and the thermodynamical potentials to be identical to those of the πp case. The parameters are determined from a fit of the CERN data [48] for $50 \leq E_{lab} \leq 300$ GeV and a $|t|$ domain between 0.0086-0.0481 GeV². We obtain a $\chi^2 = 640$ for 584 pts or a $\chi^2/pt = 1.1$ which is close to the pion-proton value. The obtained parameters for the pomeron are given in Table 6:

d_0	$=$	$0.072 \pm 0.007,$	d_1	$=$	17.98699 ± 1.03
d_2	$=$	$23.262 \pm 1.20,$	d_3	$=$	46.306 ± 2.215
b_0	$=$	0.5640 ± 0.0124 fm			

Table 6: Pomeron parameters of the Fermi model for π^\pm ^4He elastic scattering.

The parameter b_0 has the same order of magnitude as the one obtained in p ^4He . The different quarks components are plotted in Fig. 21, we see that the gluon, the quark u and the sea give the major contributions.

We show in Figs. 22-23 a plot of differential cross sections, although the t range is limited to the forward direction the agreement with data remains good. In Fig. 24 we make a prediction for the large $|t|$ π^- ^4He differential cross section at the highest measured energy 300 GeV, a dip occurs at $|t| = 0.3$ GeV², which is slightly shifted to higher $|t|$ value compared to the reaction p ^4He (see Fig. 14).

For the total cross sections we obtain at $E_{lab} = 150$ GeV a value $\sigma_{tot} = 83.6 \pm 0.2$ mb for π^- ^4He and $\sigma_{tot} = 85.17 \pm 0.3$ mb for π^+ ^4He , the experimental values are respectively $\sigma_{tot} = 83.0 \pm 0.9$ mb and $\sigma_{tot} = 85.3 \pm 0.7$ mb from Ref. [48].

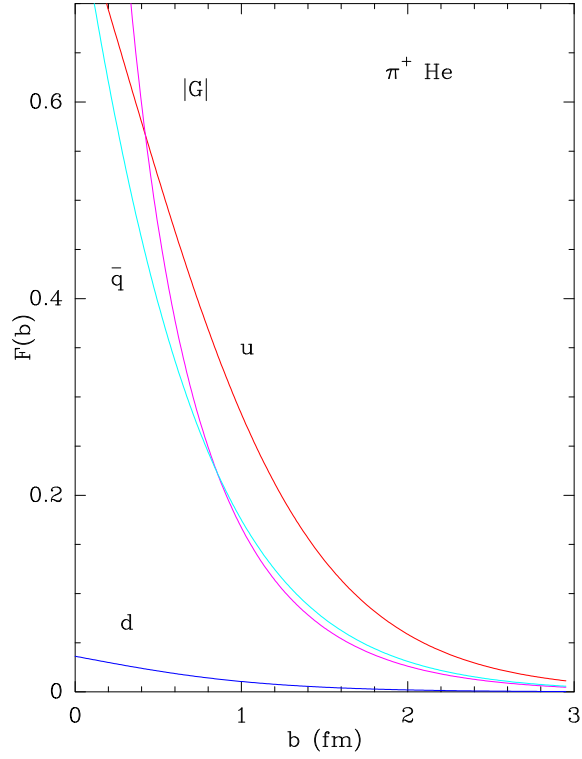


Figure 21: Individual contribution of quarks to the profile function as a function of b for $\pi^+ {}^4\text{He}$.

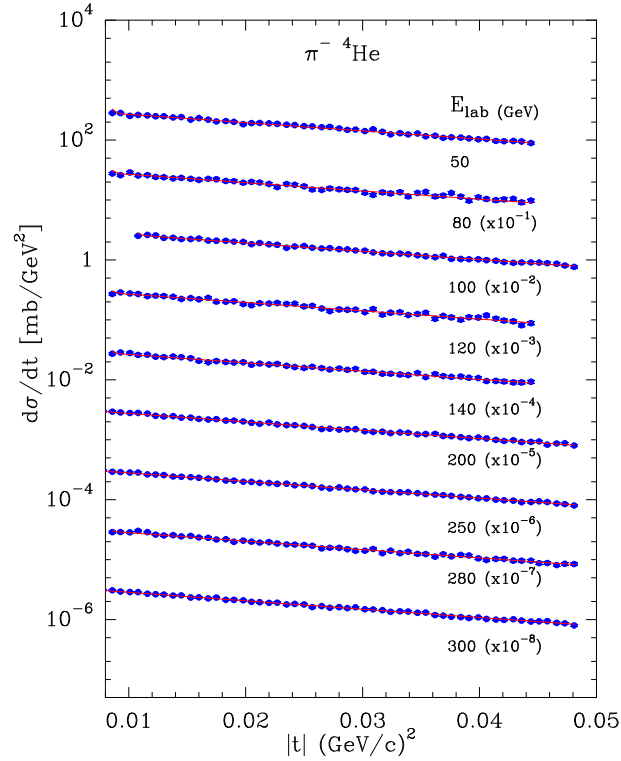


Figure 22: The $\pi^- {}^4\text{He}$ differential cross section as function of $|t|$. Experiment from Ref. [48].

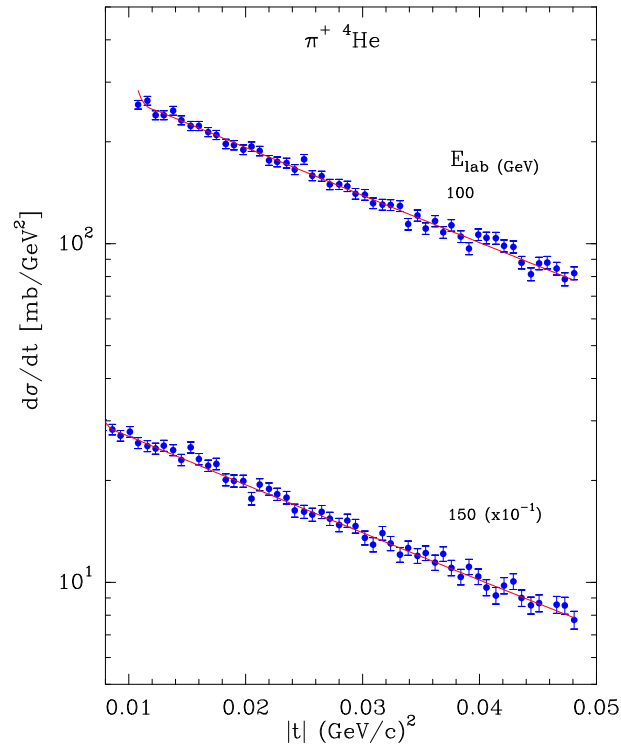


Figure 23: The $\pi^+ {}^4\text{He}$ differential cross section as function of $|t|$. Experiment from Ref. [48].

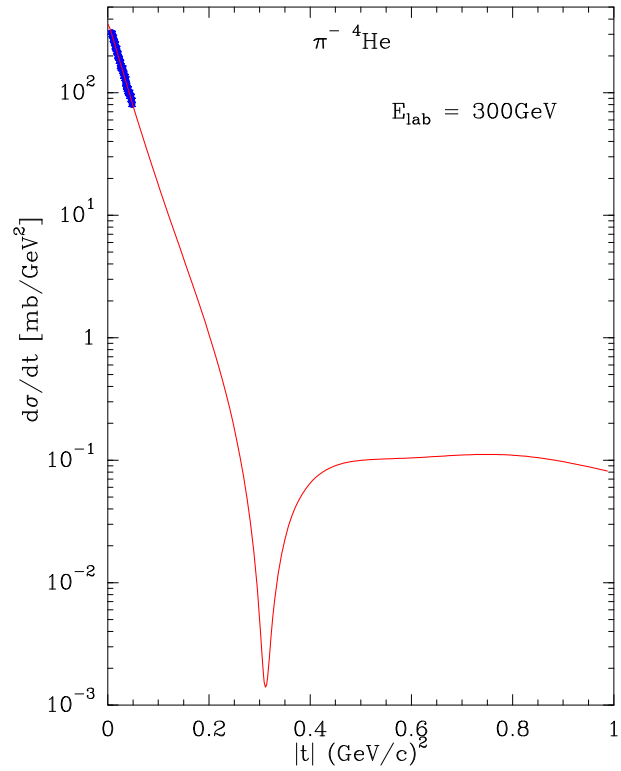


Figure 24: The $\pi^- {}^4\text{He}$ differential cross section at large $|t|$ values. Experiment from Ref. [48].

In the previous sections we made an analysis of 8 reactions, $p p, \bar{p} p, p d, p {}^4\text{He}, \pi^\pm p, \pi^\pm {}^4\text{He}$, the parameter b_0 introduced in the profile function Eqs. (10),(14) is related to the average size of the interacting partons system. We show in Fig. 25 a plot of the b_0 values as a function of the number of quarks u and d which are involved in a reaction, we observe an increase of the b_0 values with the number of quarks, an expected feature but interesting to confirm. This result is similar to the well known nuclear situation where the mean radius of a nucleus increases with the corresponding atomic mass number.

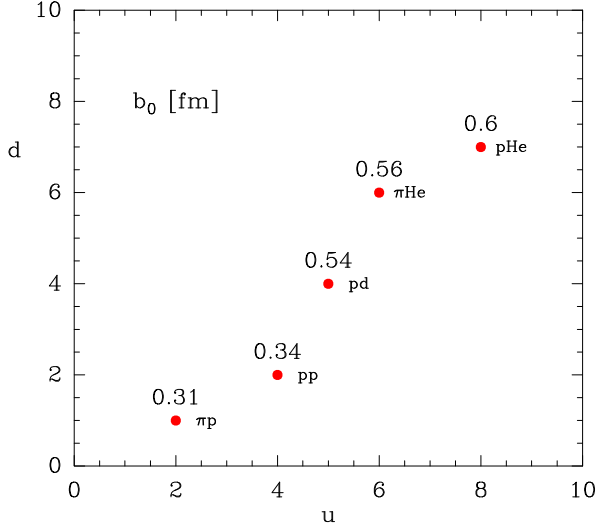


Figure 25: The b_0 values as function of u and d quarks number.

10 Conclusion

The introduction of Fermi-Dirac functions as a new opaqueness built in with different parton components in impact parameter space gives a reasonable description of 8 elastic reactions $p p, \bar{p} p, p d, p {}^4\text{He}, \pi^\pm p$ and $\pi^\pm {}^4\text{He}$. The size and the behavior of these components in impact parameter space agrees with what we expect in their localization inside the interaction domain. This first simplified approach certainly needs a more refined version by the introduction of heavy quarks and also by reducing the number of parameters.

We would like to emphasize that we do not have to rely on the assumption of proportionality between the matter distribution and the charge distribution which was introduced arbitrarily in the original BSW because in our Fermi approach the relation is obtained in a natural way. In BSW the presence of the extra term in $\tilde{F}(t)$ to cancel a second dip which was never justified is now explained by the role of the gluon. We have also proven that the thermodynamical potentials associated to the

partons and determined from the basic interactions in $p p$ and πp elastic scattering are an intrinsic property of the partons also valid for elastic light nuclei reactions.

With the same approach one could envisage an extension to the spin amplitudes, where for each parton one defines two potentials related to the spin orientation up-down, in an analogous way to the polarized PDF [9]. However, due to the scarce measurements of polarized elastic reactions at high energy there exists a difficulty to obtain reliable values of the parameters.

I am grateful to J. Soffer for constructive comments in the preparation of the manuscript.

References

- [1] C. Bourrely, J. Soffer, and T. T. Wu, Phys. Rev. D **19**, 3249 (1979).
- [2] C. Bourrely, J. Soffer, and T. T. Wu, Nucl. Phys. B **247**, 15 (1984).
- [3] C. Bourrely, J. Soffer, and T. T. Wu, Eur. Phys. J. C **28**, 97 (2003).
- [4] C. Bourrely, J. Soffer, and T. T. Wu, Eur. Phys. J. C **71**, 1061 (2011).
- [5] H. Cheng and T.T. Wu, Phys. Rev. Lett. **24**, 1456 (1970).
- [6] H. Cheng and T.T. Wu, *Expanding Protons: Scattering at High Energies*, M.I.T. Press, Cambridge, MA (1987).
- [7] T.T. Wu and C.N. Yang, Phys. Rev. **137**, B708 (1965).
- [8] T. Chou and C.N. Yang, Phys. Rev. **170**, 1591 (1968); *ibidem* **175**, 1832 (1968); Phys. Rev. Lett. **20**, 1213 (1968).
- [9] C. Bourrely, F. Buccella and J. Soffer, Eur. Phys. J. C **23**, 487 (2002); Mod. Phys. Lett. A **18**, 771 (2003); Eur. Phys. J. C **41**, 327 (2005).
- [10] M.M. Islam, R.J. Luddy and A.V. Produkin, Int. J. Mod. Phys. A **21** 1 (2006), arXiv:0508.200 [hep-ph].
- [11] P. Brogueira and J. Dias de Deus, Eur. Phys. J C **37**, 075006 (2010), arXiv:1005.3644 [hep-ph].
- [12] V. Uzhinsky and A. Galoyan, arXiv:1210.7338 [hep-ph].
- [13] J. Cleymans, 1st International Conference on New Frontiers in Physics ICFP 2012, arXiv:1210:7464 [hep-ph].
- [14] J. Cleymans, G.I. Lykasov, A.S. Parvan, A.S. Sorin, O.V. Teryaev and D. Worku, arXiv:1302.1970 [hep-ph].

- [15] I.M. Dremin, Phys. Uspekhi **56**, 3 (2013), arXiv:1206.5474 [hep-ph].
- [16] A. Biliias and A. Bzdak, Acta Phys. Pol. B **38**, 159 (2007) arXiv:0612.038 [hep-ph]. F. Nemes and T. Csörgő, J. Mod. Phys. A **27**, 1250175 (2012), arXiv:1204.5617 [hep-ph].
- [17] A.V. Belitsky and A.V. Radyushkin, Phys. Rept. **418**, 1 (2005), arXiv:0504.030 [hep-ph].
- [18] G. Antchev et al., TOTEM Collaboration, Europhys. Lett. **95**, 41001 (2011), *ibidem* **96**, 21002 (2011), CERN-PH-EP-2012-239.
- [19] A.K. Kohara, E. Ferreira and T. Kodama, arXiv:1212.3652 [hep-ph].
- [20] ATLAS/ALFA Collaboration, CERN/LHCC/2008-004,2008; P. Puzo, AIP Conf. Proc. 1105, 105 (2009).
- [21] N.A. Amos et al., Phys. Rev Lett. **68**, 2433 (1992).
- [22] F. Abe et al., Phys. Rev. D **50**, 5550 (1994).
- [23] C. Avila et al., Phys. Lett. B **537**, 41 (2002).
- [24] N. Kwak et al., Phys. Lett. B **58**, 233 (1975).
- [25] U. Amaldi et al., Nucl. Phys. B **166**, 301 (1979).
- [26] E. Nagy et al., Nucl. Phys. B **150**, 221 (1979).
- [27] A. Breakstone et al., Phys. Rev. Lett. **54**, 2180 (1985).
- [28] M. Ambrosio et al., Phys. Lett. B **115**, 495 (1982).
- [29] A. Breakstone et al., Nucl. Phys. B **248**, 253 (1984).
- [30] C. Augier et al., Phys. Lett. B **316**, 448 (1993).
- [31] F. Abe et al., Phys. Rev. D **50**, 5518 (1993).
- [32] M. Bozzo et al., Phys. Lett. B **147**, 385 (1984); Phys. Lett. B **155**, 197 (1985).
- [33] E710 Collaboration, N.M. Amos et al., Phys Lett. B **247**, 127 (1990).
- [34] CDF Collaboration, F. Abe et al., Phys. Rev. D **50**, 5518 (1993).
- [35] DØ Collaboration, V.M. Abazov et al., FERMILAB-PUB-12-263-E, arXiv:1206.0687 [hep-ex].
- [36] R.E. Breedon et al., Phys. Lett. B **216**, 459 (1989).

- [37] D. Bernard et al., Phys. Lett. B **171**, 142 (1986).
- [38] Particle Data Group, <http://pdg.lbl.gov>.
- [39] X. Zhan, Ph.D. thesis, Massachusetts Institute of Technology, (January 2010), arXiv:1108.4441[nucl-ex]; X. Zhan et al., Phys. Lett. B **705**, 59 (2011).
- [40] Ch. Berger et al., Phys. Lett. B **35**, 85 (1971).
- [41] K.M. Hanson et al., Phys. Rev. D **8**, 753 (1973).
- [42] J. Arrington, W. Melnitchouk and J.A. Tron, Phys. Rev. C **76**, 035205 (2007).
- [43] A.S. Carroll et al., Phys. Lett. B **80**, 423 (1979).
- [44] Y. Akimov et al., Phys. Rev. D **12**, 3399 (1975).
- [45] G.G. Beznogikh et al., Phys. Lett. B **43**, 85 (1973).
- [46] D. Gross et al., Phys. Rev. Lett. **41**, 217 (1978).
- [47] A. Bujak et al., Phys. Rev. D **23**, 1895 (1981).
- [48] J.P. Burq et al., Nuc. Phys. B **187**, 205 (1981).
- [49] C.W. Akerlof et al., Phys. Rev. D **14**, 2864 (1976).
- [50] R. Rubinstein et al., Phys. Rev. D **30**, 1413 (1984).
- [51] R. Cool et al., Phys. Rev. D **24**, 2821 (1981).
- [52] A. Schiz et al., Phys. Rev. D **24**, 26 (1979).
- [53] M. Adamus et al., Phys. Lett. B **186**, 223 (1987).